Acoustofluidics: theory and simulation of radiation forces at ultrasound resonances in microfluidic devices

Barnkob, Rune; Bruus, Henrik

Published in:
Proceedings of Meeting on Acoustics

Link to article, DOI:
10.1121/1.3186746

Publication date:
2009

Document Version
Publisher's PDF, also known as Version of record

Proceedings of Meetings on Acoustics

Volume 6, 2009 http://asa.aip.org

157th Meeting
Acoustical Society of America
Portland, Oregon
18 - 22 May 2009
Session 2pBB: Biomedical Ultrasound/Bioresponse to Vibration

2pBB2. Acoustofluidics: theory and simulation of radiation forces at ultrasound resonances in microfluidic devices

Rune Barnkob and Henrik Bruus*

***Corresponding author's address: Department of Micro- and Nanotechnology, Technical University of Denmark, DTU Nanotech, Building 345 east, Kongens Lyngby, 2800, -, Denmark, Henrik.Bruus@nanotech.dtu.dk**

Theoretical analysis is combined with numerical simulations to optimize designs and functionalities of acoustofluidic devices, i.e. microfluidic devices in which ultrasound waves are used to anipulate biological particles. The resonance frequencies and corresponding modes of the acoustic fields are calculated for various specific geometries of glass/silicon chips containing water-filled microchannels. A special emphasis is put on taking the surrounding glass/silicon material into account, thus going beyond the traditional transverse half-wavelength picture. For the resonance frequencies, where the largest possible acoustic powers are obtained in the microfluidic system, the time-averaged acoustic radiation force on single particles is determined. Schemes for in situ calibration of this force are presented and discussed.

Published by the Acoustical Society of America through the American Institute of Physics

 [DOI: 10.1121/1.3186746]
Received 27 May 2009; published 6 Jul 2009

1. INTRODUCTION

The studies of acoustic radiation forces on particles have a long history. The analysis of incompressible particles in acoustic fields dates back to the work in 1934 by King [1], while the forces on compressible particles were calculated in 1955 by Yosioka and Kawasima [2]. Their work was admirably summarized in 1962 in a short paper by Gorkov [3]. The use of ultrasound standing waves for particle manipulation and separation has received renewed interest in the past decade since its application in the emerging field microfluidics [4]–[20].

In these recent papers, standing ultrasound resonances have been established in flat microfluidic channels of height $h \approx 150\ \mu$m, width $w \approx 400\ \mu$m, and length $\ell \approx 4$ cm embedded in a silicon/glass chip with an area several square centimeter large and a height $H \approx 1$ mm. A wide spread assumption is that due to the large acoustic impedance ratio of the order of 13 between silicon/glass and water, the leading resonance at frequency f is given by the half-wavelength condition $\lambda/2 = c_{\mathrm{wa}}/(2f) = w$. This leads to $f \approx 2$ MHz. This is of course not exactly true. By taking the whole silicon/glass/water resonator into account, we study theoretically the deviations from this idealization to be expected in actual devices.

Another particular problem with the application of standing ultrasound waves in microfludic systems concerns the calibration of the acoustic radiation force. Acoustic power sent from the actuator to the microfluidic system suffers losses due to heating in the system and acoustic radiation to the surroundings. These losses are hard to measure, and at the same time it is difficult to mount pressure sensors inside the microfluidic system for direct determination of the acoustic power actually present. We present a possible *in situ* calibration of the acoustic radiation force from a standing ultrasound wave on suspended spherical particles in a microfluidic channel. The method relies on determining the critical flow velocity above which the particles cease to be trapped by the ultra sound forces.

2. BACKGROUND THEORY

Linear acoustics and acoustic radiation forces are treated in many textbooks. Basic theory can be found in Lighthill [21] and theoretical aspect of acoustics in microfluidics, acoustofluidics, can be found in Bruus [22]. In this work we rely on the formulation of Gorkov [3].

2.1. Governing equations and boundary conditions

We consider a silicon/glass chip containing a microchannel filled with an aqueous solution of particles. A piezo actuator is glued to the chip, such that when applying an AC voltage at MHz frequency, the piezo element vibrates and induces a time-harmonic ultrasound pressure field $p_1 \exp(-\mathrm{i}\,\omega t)$, where $\omega = 2\pi f$ is the angular frequency and f the frequency. Here, we use the complex representation of the harmonic time dependence. In the following the time-harmonic factor is implicitly assumed, and we just write the amplitude p_1. Likewise for the velocity field $\boldsymbol{v}_1$ of the carrier liquid.

Before the onset of the external ultrasound field the solution is in a quiescent state at constant uniform pressure p_{wa} and zero velocity. The viscosity of the carrier liquid has a negligible influence on the acoustic radiation forces. Consequently, to a good approximation, the pressure field p_1 and velocity field $\boldsymbol{v}_1$ inside the chip and the microchannel are governed by simple linear acoustics of inviscid fluids, i.e. the Helmholtz wave equation for the pressure and potential flow for the velocity,

$$\nabla^2 p_1 = -\frac{\omega^2}{c_{\mathrm{wa}}^2}\, p_1, \tag{1a}$$

$$\boldsymbol{v}_1 = -\frac{\mathrm{i}}{\omega \rho_{\mathrm{wa}}} \boldsymbol{\nabla} p_1. \tag{1b}$$

Here, c_{wa} and ρ_{wa} is the speed of sound and the density of the carrier liquid, respectively. Note that in this simple model we neglect the shear waves in the solids.

At a boundary characterized by the surface normal vector $\boldsymbol{n}$, we employ three different boundary conditions in this work: the hard wall (zero velocity) condition, the soft wall (zero pressure) condition, and the continuity condition for

TABLE 1. Physical parameters used in the model for polystyrene beads in water inside a silicon chip.

Speed of sound, water	c_{wa}	1483 $\mathrm{m\,s^{-1}}$	Density, water	ρ_{wa}	998 $\mathrm{kg\,m^{-3}}$
Speed of sound, silicon	c_{si}	8490 $\mathrm{m\,s^{-1}}$	Density, silicon	ρ_{si}	2331 $\mathrm{kg\,m^{-3}}$
Speed of sound, pyrex	c_{py}	5647 $\mathrm{m\,s^{-1}}$	Density, pyrex	ρ_{ps}	2230 $\mathrm{kg\,m^{-3}}$
Speed of sound, polystyrene	c_{ps}	1700 $\mathrm{m\,s^{-1}}$	Density, polystyrene	ρ_{ps}	1050 $\mathrm{kg\,m^{-3}}$
Speed of sound ratio $c_{\mathrm{ps}}/c_{\mathrm{wa}}$	β_{ps}	1.15	Density ratio $\rho_{\mathrm{ps}}/\rho_{\mathrm{wa}}$	γ_{ps}	1.05
Compressibility factor, polystyrene	f_1	0.276	Density factor, polystyrene	f_2	0.034

pressure and velocity across interior boundaries,

$$\boldsymbol{n}\cdot\boldsymbol{\nabla}p_1 = 0, \qquad \text{(hard wall)}, \tag{2a}$$

$$p_1 = 0, \qquad \text{(soft wall)}, \tag{2b}$$

$$\frac{1}{\rho_a}\boldsymbol{n}\cdot\boldsymbol{\nabla}p_1^{(a)} = \frac{1}{\rho_b}\boldsymbol{n}\cdot\boldsymbol{\nabla}p_1^{(b)}, \quad \text{and} \quad p_1^{(a)} = p_1^{(b)}, \quad \text{(continuity)}. \tag{2c}$$

2.2. Acoustic resonances

The acoustically soft water inside the channel surrounded by the acoustically hard silicon/glass chip forms an acoustic cavity. This implies that acoustic resonances occur for certain specific frequencies ω_j, $j = 1,2,3,\ldots$. An acoustic resonance at frequency ω_j is a state where the average acoustic energy density inside the cavity is several orders of magnitude larger than at other frequencies $\omega \neq \omega_j$. By tuning the applied frequency to one of these resonance frequencies, the acoustic forces become so strong that they in a reliable way can be used to manipulate particles suspended in the carrier liquid.

The exact values of the resonance frequencies ω_j depend on the geometry of the acoustic cavity and of the material parameters of the liquid in the cavity as well as the surrounding material. Specifically, the relevant material parameters are the speed of sound c_{wa} and density ρ_{wa} of the water and likewise the speed of sound c_{si} and density ρ_{si} of the silicon chip, see Table 1. In the general case, the resonance frequencies can only be calculated using numerical methods, however, in few cases they may be found analytically.

For a rectangular channel of length l, width w, and height h, surrounded by an acoustically infinitely hard material, the resonance frequencies may be found analytically. This case approximates our experimental system reasonably well. Neglecting the inlet and outlet, our microchannel is indeed rectangular. Moreover, since the parameters listed in Table 1 yields an acoustic impedance ratio $(\rho_{\mathrm{si}}c_{\mathrm{si}})/(\rho_{\mathrm{wa}}c_{\mathrm{wa}}) = 13.4$ much larger than unity, the silicon surrounding our rectangular water channel can to a good approximation be treated as an infinitely hard material. In that case the normal velocity on all walls is zero, which according to Eq. (1b) is equivalent to Neumann boundary conditions $\boldsymbol{n}\cdot\boldsymbol{\nabla}p_1 = 0$ for the pressure. It is easily verified that with this boundary condition the pressure p_1 solving Eq. (1a) for a rectangular box placed along the coordinate axes with its opposite corners at $(0,0,0)$ and (l,w,h) is

$$p_1(x,y,z) = p_{\mathrm{a}}\cos(k_x x)\cos(k_y y)\cos(k_z z), \quad \text{with} \quad k_j = n_j\frac{\pi}{L_j}, \quad n_j = 0,1,2,3,\ldots \tag{3}$$

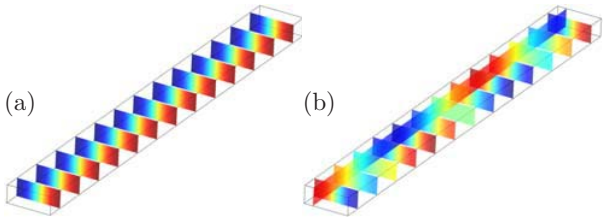

FIGURE 1. Color plot (red positive, blue negative) of the pressure field p_1 at resonance in a water-filled microchannel of length $l = 5$ mm along x, width $w = 0.5$ mm along y, and height $h = 0.2$ mm along z, surrounded by an infinitely hard acoustic material, see Eq. (3). (a) Resonance $(n_x,n_y,n_z) = (0,1,0)$ with $f_{0,1,0} = 1.48$ MHz, and (b) $(n_x,n_y,n_z) = (3,1,0)$ with $f_{3,1,0} = 1.55$ MHz.

where p_a is the pressure amplitude, and where $L_x = l$, $L_y = w$, and $L_z = h$. The corresponding three-index resonance frequencies $f_{n_x,n_y,n_z} = \omega_{n_x,n_y,n_z}/(2\pi)$ are given by

$$f_{n_x,n_y,n_z} = \frac{c_\mathrm{wa}}{2}\sqrt{\frac{n_x^2}{l^2}+\frac{n_y^2}{w^2}+\frac{n_z^2}{h^2}}, \quad \text{with} \quad n_x,n_y,n_z = 1,2,3,4,\ldots. \tag{4}$$

Two examples of resonant standing ultrasound waves are shown in Fig. 1.

2.3. The acoustic radiation force

Given the acoustic pressure field p_1 and velocity field $\boldsymbol{v}_1$ it is possible to calculate the acoustic radiation force on a particle with volume V and linear dimension $V^{\frac{1}{3}}$ much smaller than the acoustic wavelength λ. Both for biological cells and for micrometric tracer particles we are in this limit. The material parameters, with subscripts "wa" for the water and "p" for the particle, enter as the speed of sound ratio β and the density ratio γ,

$$\beta = \frac{c_\mathrm{p}}{c_\mathrm{wa}}, \qquad \gamma = \frac{\rho_\mathrm{p}}{\rho_\mathrm{wa}}, \tag{5}$$

which appear in the pre-factors f_1 and f_2 as

$$f_1 = 1 - \frac{1}{\gamma\beta^2}, \qquad f_2 = \frac{2\gamma-2}{2\gamma+1}. \tag{6}$$

The general expression for the time-averaged acoustic radiation force $\boldsymbol{F}_\mathrm{ac}$ is given by Gorkov [3],

$$\boldsymbol{F}_\mathrm{ac} = -V\boldsymbol{\nabla}\left[\frac{f_1}{2\rho_\mathrm{wa}c_\mathrm{wa}^2}\langle p_1^2\rangle - \frac{3f_2\rho_\mathrm{wa}}{4}\langle|\boldsymbol{v}_1|^2\rangle\right] = -\frac{V}{4\rho_\mathrm{wa}c_\mathrm{wa}^2}\boldsymbol{\nabla}\left[2f_1\langle p_1^2\rangle - 3f_2\frac{1}{k^2}\langle|\boldsymbol{\nabla}p_1|^2\rangle\right], \tag{7}$$

where the latter form is obtained by use of Eq. (1b) and $k^2 = k_x^2 + k_y^2 + k_z^2$.

3. ANALYSIS OF TRANSVERSE HALF-WAVELENGTH MODES

For experimental applications it is desirable to work with half-wavelength waves of odd symmetry in the transverse y-direction of the water-filled channel, i.e. $w = \lambda/2$ and thus a resonance frequency $f_{0,1,0} \approx c_\mathrm{wa}/(2w)$. For such modes the acoustic radiation force focuses hard particles at the pressure node in the vertical xz-plane along the center line of the channel, see Fig. 1(a). The question now arises how the width W of surrounding silicon chip affects this simple estimate for $f_{0,1,0}$.

3.1. Analysis of 1D models

In Fig. 2 is sketched a 1D model for the transverse y-direction, where for simplicity we introduce the lengths $a \equiv w/2$ and $b \equiv (W-w)/2$ for half the width of the channel and the width of the silicon chip from the channel to the edge, respectively. The model is symmetric around the center of the channel thus leading to two classes of solutions for the pressure, namely even and odd modes.

Using the proper symmetry boundary condition at $y = -a$, either Eq. (2a) for even or Eq. (2b) for odd modes, and the soft boundary condition Eq. (2b) at $y = b$, results in cosine (even) or sine (odd) solutions for the pressure waves,

$$p_\mathrm{wa}(y) = A_\mathrm{wa}\cos\left[k_\mathrm{wa}(y+a)\right], \quad \text{(even)}, \tag{8a}$$
$$p_\mathrm{wa}(y) = A_\mathrm{wa}\sin\left[k_\mathrm{wa}(y+a)\right], \quad \text{(odd)}, \tag{8b}$$
$$p_\mathrm{si}(y) = A_\mathrm{si}\sin\left[k_\mathrm{si}(y-b)\right], \tag{8c}$$

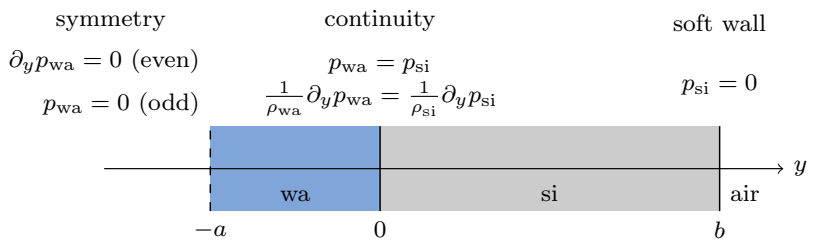

FIGURE 2. Sketch of the 1D model containing half the water-filled channel (wa) and the silicon chip (si). The model includes three boundaries; a symmetric point in the center of the channel ($y = -a$), an interface between channel and chip ($y = 0$), and the outer boundary of the silicon chip ($y = b$). Notice that the boundary condition at the symmetry point gives either even or odd pressure-modes across the channel.

where $A_{\rm wa}$ and $A_{\rm si}$ are pressure amplitudes. Employing the continuity condition Eq. (2c) at $y = 0$ and utilizing that $k_{\rm si} = k_{\rm wa} c_{\rm wa}/c_{\rm si}$, results in transcendental equations for even and odd pressure eigenmodes

$$\cot(\theta) = z\tan(\alpha\theta), \quad \text{(even)}, \qquad \text{and} \qquad \cot(\theta) = -\frac{1}{z}\cot(\alpha\,\theta), \quad \text{(odd)}, \tag{9}$$

where $\theta = k_{\rm wa} a$ is the dimensionless wavenumber, $z = (\rho_{\rm si} c_{\rm si})/(\rho_{\rm wa} c_{\rm wa}) \approx 13.4$ is the acoustic impedance ratio, and α is the aspect ratio parameter given by

$$\alpha \equiv \frac{c_{\rm wa}}{c_{\rm si}}\frac{b}{a} = \frac{\text{number of wavelengths in the silicon chip}}{\text{number of wavelengths in the water channel}}. \tag{10}$$

From Eq. (9) it is now possible for a given value of α to determine which value of $k_{\rm wa} = 2\pi/\lambda_{\rm wa}$ that most accurately approximates a perfect half-wavelength mode $\lambda^*_{\rm wa} = 4a$ in the water-filled channel. Expressing the actual wavelength $\lambda_{\rm wa}$ as a function of the ideal wavelength $\lambda^*_{\rm wa}$ and a relative shift δ in the wavelength, we get

$$\lambda_{\rm wa} = \lambda^*_{\rm wa}(1+\delta). \tag{11}$$

For a perfect half-wavelength mode we have $\theta = \pi/2$, and the relative shift in wavelength is zero, $\delta = 0$.

In Fig. 3 is shown a graphic representation of the even and odd pressure eigenmode solutions for $\alpha = 1$ and 2. The perfect half-wavelength solution, $\theta/\pi = 0.5$ is odd in the case of $\alpha = 1$ (marked A) and even for $\alpha = 2$ (marked B). In the latter case two odd solutions (marked $\rm C_-$ and $\rm C_+$) are nearly half-wavelength modes with values of θ/π close to 0.5. The actual pressure modes $p(y)$ for the four cases A, B, $\rm C_+$, and $\rm C_-$ are shown in Fig. 4.

A quantitative measure of the quality of a given eigenmode can be obtained from the expression for the acoustic energy density $\mathscr{E}$,

$$\mathscr{E}(\boldsymbol{r}, f) = \frac{1}{4\rho(\boldsymbol{r})}\left[\frac{1}{(2\pi f)^2}\,|\boldsymbol{\nabla} p_1(\boldsymbol{r})|^2 + \frac{1}{c^2}\,|p_1(\boldsymbol{r})|^2\right]. \tag{12}$$

The higher the average acoustic energy density $\langle \mathscr{E}_{\rm wa} \rangle$ is in the water-filled channel relative to the maximum acoustic energy density $\mathscr{E}^{\rm max}_{\rm si}$ in the surrounding silicon chip, the better. For the four specific modes A, B, $\rm C_+$, and $\rm C_-$ shown in Fig. 4 we find numerically that $\langle \mathscr{E}_{\rm wa} \rangle / \mathscr{E}^{\rm max}_{\rm si} = 76.5$, 0.4, 10.6, and 10.6, respectively. Clearly, the perfect anti-symmetric half-wavelength mode in the $\alpha = 1$ chip has the best figure of merit.

3.2. Analysis of 2D models

We now extend our analysis of the half-wavelength modes from 1D to 2D by taking the length direction of the system along the x-axis into account on top of the transverse direction along the y-axis. As shown in Fig. 5, the most prominent change from 1D to 2D is the appearance of oscillations in the axial direction along the x-axis, a feature not possible in 1D. The third dimension can be neglected due to the absence of dynamics in this direction for channels with a height less than half a wavelength [17].

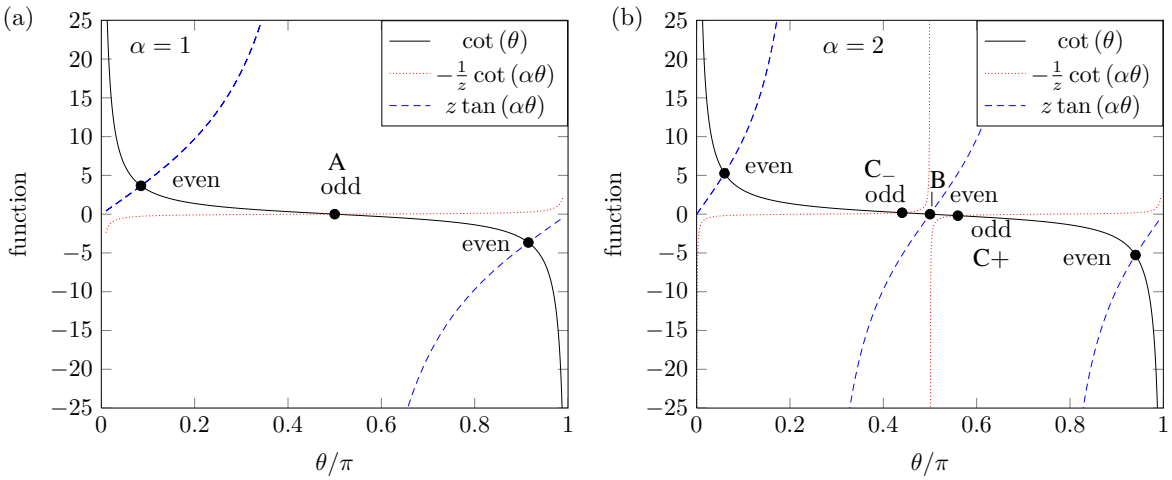

FIGURE 3. Graphic representation of the even and odd pressure eigenmode solutions in the 1D silicon/water model to the transcendental equations given in Eq. (9) for (a) $\alpha = 1$ and (b) $\alpha = 2$. The perfect half-wavelength solution, $\theta/\pi = 0.5$ is odd in the case of $\alpha = 1$ (marked A) and even for $\alpha = 2$ (marked B). In the later case two odd solutions (marked C_- and C_+) are nearly half-wavelength modes with values of θ/π close to 0.5.

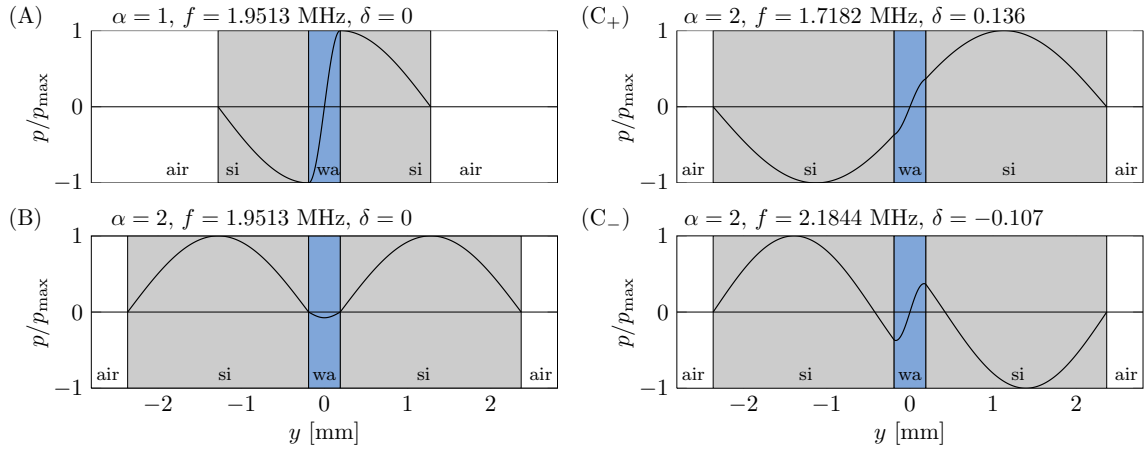

FIGURE 4. Pressure eigenmodes $p(y)$ of the four special cases marked in Fig. 3 for the 1D silicon/water (gray/blue) model given a water channel width of $w = 2a = 0.38$ mm. (A) The perfectly matched silicon chip with $\alpha = 1$ supporting the anti-symmetric half-wavelength pressure mode in the water channel at frequency $f = 1.9513$ MHz. (B) The silicon chip with $\alpha = 2$ also supports a pressure eigenmode at $f = 1.9513$ MHz, however this mode is symmetric. (C_+) An anti-symmetric eigenmode in the $\alpha = 2$ chip with a frequency as close as possible, but lower, to the ideal frequency of panel (A). Here $f = 1.7182$ MHz and the wavelength in the water channel is 13.6% too long ($\delta = 0.136$). (C_-) An anti-symmetric eigenmode in the $\alpha = 2$ chip with a frequency as close as possible, but higher, to the ideal frequency of panel (A). Here $f = 2.1844$ MHz and the wavelength in the water channel is 10.7% too short ($\delta = -0.107$).

As in 1D we also in 2D study the $\alpha = 1$ and $\alpha = 2$ chips. To enable direct comparison we reuse the 1D widths in 2D for the transverse y-direction. Some of the resulting pressure eigenmodes are shown in Fig. 5. We note how the modes (A), (B), (C_+), and (C_-) from the 1D case in Fig. 4 also can be identified in the 2D case of Fig. 5. However, due to the extra degree of freedom for oscillations in the axial x-direction, it is now possible even in the "bad" $\alpha = 2$ chip to find eigenmodes (D_+ and D_-), which are both close to the ideal frequency $f = 1.95$ MHz of the $\alpha = 1$ chip in panel (A) and at the same time possess the wanted odd (one-node) symmetry in the transverse y-direction. The only drawback is the appearance of several nodes in the axial direction. It is found experimentally that pressure modes with

a lower number of axial nodes lead to higher separation efficiencies [18].

As in the 1D case, we can study the quality of the 2D pressure eigenmodes by evaluating the ratio of the acoustic energy density in the water channel relative to that in the silicon chip. The results are listed in Table 2. Again, the perfectly matched A-mode has the best figure of merit, however it is seen that also the new D_+ and D_- also perform well. These three modes have high energy density ratios of 39.2, 32.0 and 36.1, respectively, while the other three modes have ratios around 6 or lower.

A natural extension of the model is a many-channel chip, which supports higher flow rates. We reuse the former channel geometries to create a chip with eight parallel channels. Resulting modes for two chips of different values of α are shown in Fig. 6. We note the obvious different in homogeneity in pressure amplitudes from the perfectly matching mode in the $\alpha = 1$ chip to the badly matching mode in the arbitrarily chosen $\alpha = 0.47$ chip. Regarding the energy ratios, the perfectly matching chip mode has an homogeneous average energy density ratio of 39.4, whereas the mode in the non-matching chip has an inhomogeneous energy density with an average ratio of 16.4. The two examples

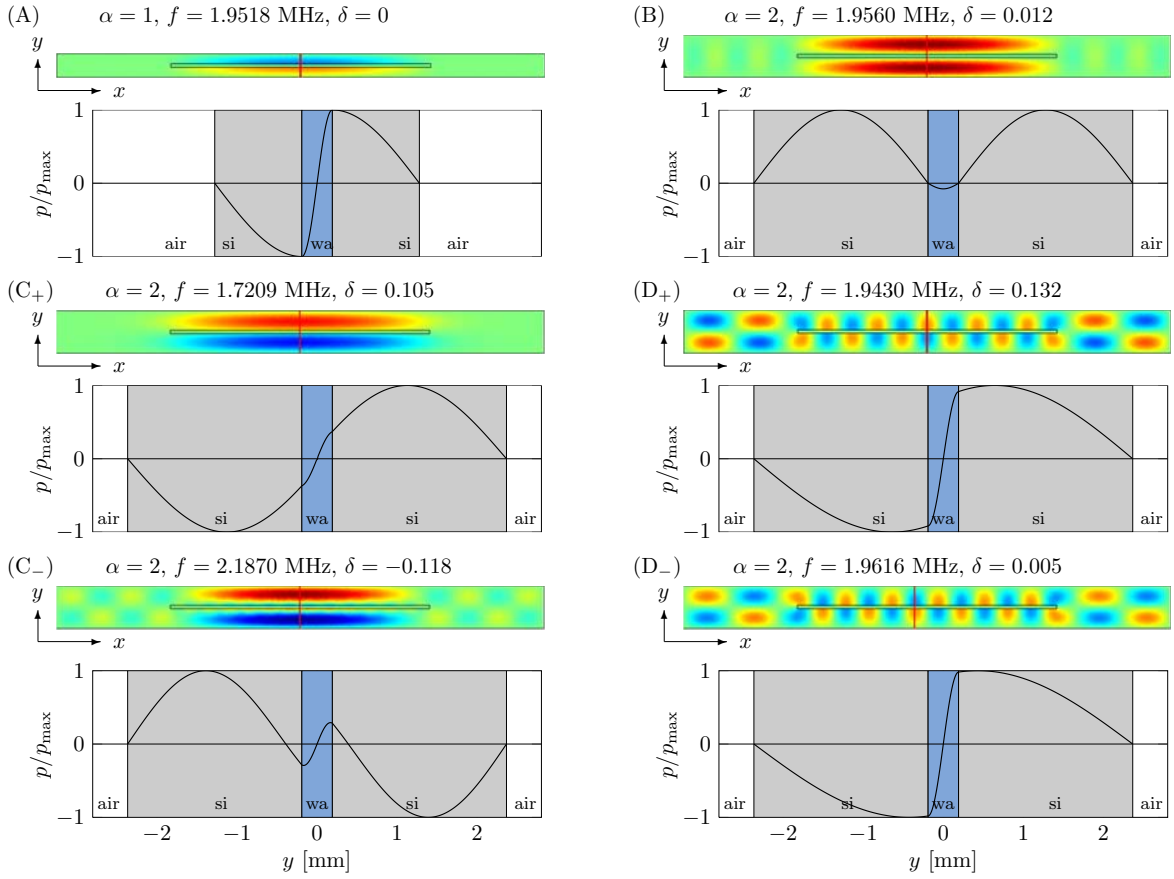

FIGURE 5. 2D COMSOL simulations of six pressure eigenmodes in a water-filled channel (wa/blue) of width $w = 0.38$ mm and length $l = 29.30$ mm. The channel is placed in a silicon chip (si/gray) of width $W = \alpha\,(c_{\rm si}/c_{\rm wa})w$ and length $L = 55.00$ mm. The widths here are as in the 1D system of Fig. 4. For each mode the pressure amplitude is plotted along the indicated red line in the corresponding 2D color plot of the pressure amplitude. (A) $\alpha = 1$, $W = 2.6$ mm: perfectly matching mode at the ideal frequency $f = 1.95$ MHz having odd (one-node) transverse symmetry and even (zero-node) axial symmetry. (B) $\alpha = 2$, $W = 4.7$ mm: matching mode at $f = 1.95$ MHz very near the ideal frequency, but having the un-wanted even (two-node) transverse symmetry and even (zero-node) axial symmetry. (C_+) and (C_-) $\alpha = 2$, $W = 4.7$ mm: as in Fig. 4 non-matching modes with frequencies far below/above the ideal frequency having the wanted odd (one-node) transverse symmetry and even (zero-node) axial symmetry. (D_+) and (D_-) $\alpha = 2$, $W = 4.7$ mm: almost matching modes with frequencies near the ideal frequency having the wanted odd (one-node) transverse symmetry, but with many nodes in the axial direction.

TABLE 2. Data for the six 2D pressure eigenmodes shown in Fig. 5. Listed are the value of the aspect parameter α and the symmetries, as well as the resulting frequency f, relative shift in wavelength δ, and energy density ratio obtained by COMSOL simulations.

Mode	α	x-symm.	y-symm.	f [MHz]	δ [%]	$\langle \mathscr{E}_{\mathrm{wa}} \rangle / \mathscr{E}_{\mathrm{si}}^{\max}$
A	1	even	odd	1.9518	0.0	39.2
B	2	even	even	1.9560	1.2	0.2
C_+	2	even	odd	1.7209	13.4	6.3
C_-	2	even	odd	2.1870	-11.7	5.1
D_+	2	even	odd	1.9430	1.4	32.0
D_-	2	odd	odd	1.9616	0.5	36.1

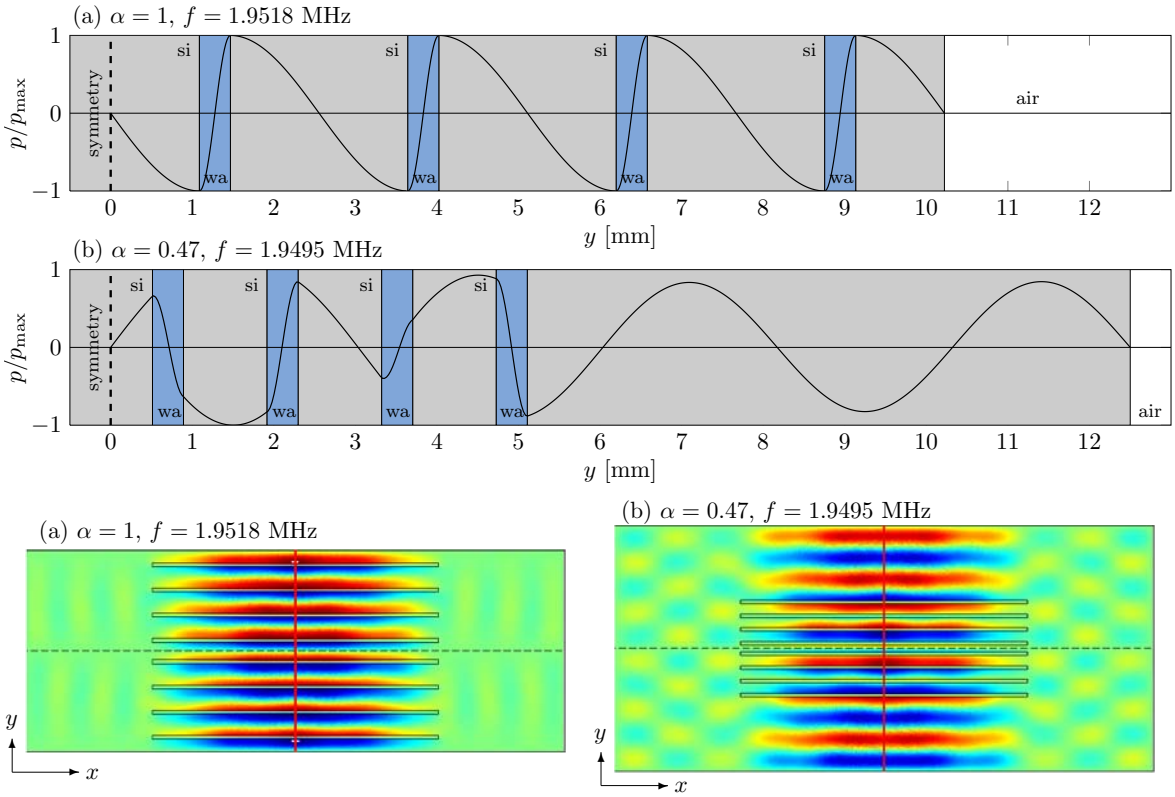

FIGURE 6. 2D COMSOL simulations of silicon chips (si/gray) length $L = 55.00$ mm containing eight parallel water-filled channels (wa/blue) each of width $w = 0.38$ mm and length $l = 29.30$ mm. Two chips are shown; (a) $\alpha = 1$ between channels and to the silicon edge, and (b) $\alpha = 0.47$ between channels and $\alpha = 6.80$ to the silicon edge. For each shown resonance the pressure amplitude is plotted as a surface plot showing the entire chip and as a symmetric cross-sectional plot along the transverse y-direction. For each plot the pressure is normalized to the maximum pressure for that given mode.

presented clearly demonstrate the importance of designing the chip surrounding the water-filled channel properly.

4. IN SITU CALIBRATION OF ACOUSTIC RADIATION FORCES ON PARTICLES

When applying standing ultrasound waves in microfludic systems, it is difficult to measure or calibrate the acoustic radiation force exerted on a particle in solution. Acoustic power sent from the actuator to the microfluidic system suffers losses due to heating in the system and acoustic radiation to the surroundings. These losses are hard to measure,

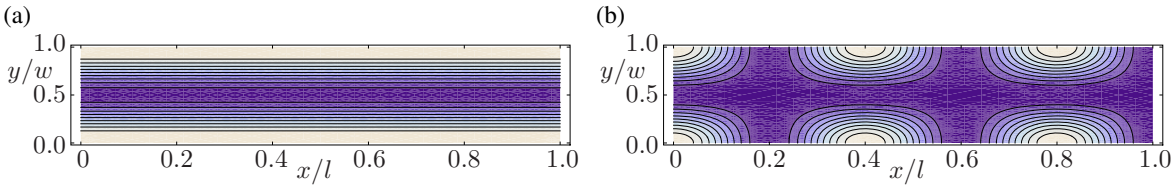

FIGURE 7. (a) Contour plot with 10% contour lines from low (dark) to high (light) of the normalized acoustic potential $U_{\mathrm{ac}}/U_{\mathrm{o}}$ from Eq. (15b) for a polystyrene sphere in water given the ideal 1D pressure field p_1 of Eq. (13a) with $(k_x,k_y)=(0,\pi y/w)$ so that $\theta=90^\circ$. (b) Similar plot for the 2D pressure field with $(k_x,k_y)=(\pi/(2w),\pi/w)$ so that $\theta\approx 63^\circ$. Further parameter values used in the simulation are given in Table 1.

and at the same time it is difficult to mount pressure sensors inside the microfluidic system for direct determination of the acoustic power actually present. Based on the insight obtained above, regarding the global wave nature of the pressure eigenmodes, we present in the following a possible chip design for *in situ* calibration of the acoustic radiation force from a standing ultrasound wave on suspended spherical particles in a microfluidic channel. The method relies on determining the critical flow velocity above which the particles cease to be trapped by the ultrasound forces.

4.1. The acoustic potential experienced by a particle

According to Eq. (7), the acoustic force acting on a particle in solution can be calculated once the pressure eigenmode p is known. Our previous analysis for straight 2D channels of length l and width w have shown that to a good approximation these eigenmodes are given by simple cosine/sine standing waves in a water channel surrounded by infinitely hard walls. Such an idealized 2D pressure eigenmode is given by

$$p_1(x,y,z) = +p_{\mathrm{a}}\cos(k_x x)\cos(k_y y), \tag{13a}$$

$$\boldsymbol{\nabla} p_1(x,y,z) = -k_x p_{\mathrm{a}}\sin(k_x x)\cos(k_y y)\boldsymbol{e}_x - k_y p_{\mathrm{a}}\cos(k_x x)\sin(k_y y)\boldsymbol{e}_y, \tag{13b}$$

$$\boldsymbol{k} = k_x\boldsymbol{e}_x + k_y\boldsymbol{e}_y. \tag{13c}$$

This standing wave can be interpreted as the result of two counter-propagating waves along the direction $\boldsymbol{k}$, which forms the angle θ with the x-axis,

$$\cos\theta = \frac{k_x}{k}, \quad \sin\theta = \frac{k_y}{k}, \quad k = \sqrt{k_x^2+k_y^2}. \tag{14}$$

Inserting this in Gorkov's expression Eq. (7), we find the acoustic force as minus the gradient of a potential U_{ac},

$$\boldsymbol{F}_{\mathrm{ac}} = -\boldsymbol{\nabla} U_{\mathrm{ac}}, \tag{15a}$$

where the acoustic potential U_{ac} and its amplitude U_{o} are given by

$$U_{\mathrm{ac}} = U_{\mathrm{o}}\Big[2f_1\cos^2(k_x x)\cos^2(k_y y) - 3f_2\sin^2(k_x x)\cos^2(k_y y)\cos^2\theta - 3f_2\cos^2(k_x x)\sin^2(k_y y)\sin^2\theta\Big], \tag{15b}$$

$$U_{\mathrm{o}} = \frac{p_{\mathrm{a}}^2 V}{8\rho_{\mathrm{wa}}c_{\mathrm{wa}}^2}. \tag{15c}$$

Two numerical examples of the acoustic potential U_{ac} for a polystyrene sphere are shown in Fig. 7.

4.2. Chip design for in situ calibration of the acoustic radiation force

The acoustic radiation force on a suspended particle can be calibrated *in situ* if it is anti-parallel to the Stokes drag force from the flow of the carrier liquid along the x-direction. By gradually increasing the flow velocity v from zero,

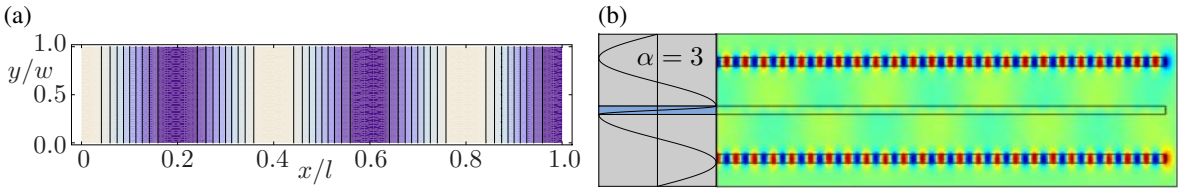

FIGURE 8. (a) Contour plot with 10% contour lines from low (dark) to high (light) of the normalized acoustic potential $U_{\mathrm{ac}}^{\mathrm{calib}}/U_{\mathrm{o}}$ from Eq. (16a) for a polystyrene sphere in water given the pressure field $p_1 = p_{\mathrm{a}}\cos(\pi x/2w)$. The parameter values are given in Table 1, and moreover $k_x = \pi/(2w)$ while $k_y = 0$ so that $\theta = 0$. (b) Color plot of the pressure eigenmode in the triple-channel $\alpha = 3$ chip. A transverse potential, as in panel (a), suitable for *in situ* acoustic force calibration is set up in the two side channels, while the center channel supports a transverse mode of odd symmetry as in Fig. 5(D_+). The left insert shows the single-channel $\alpha = 3$ chip. Note the two anti-nodes in the silicon chip (gray) above and below the water-filled channel (blue).

a critical value v^* of v can be determined, above which the acoustic radiation force no longer can trap the particle. At this point $|\boldsymbol{F}_{\mathrm{ac}}| \approx 6\pi\eta a v^*$, and the unknown pre-factor U_{o} can be determined. The calibration setup requires that $\boldsymbol{k}$ and $\boldsymbol{e}_x$ are parallel, thus $k_x \neq 0$ while $k_y = 0$. By combining Eqs. (6) and (15) with this form of the wave vector, we obtain the acoustic potential and the associated radiation force for calibration purposes on the form

$$U_{\mathrm{ac}}^{\mathrm{calib}} = U_{\mathrm{o}}\left[2f_1\cos^2(k_x x) - 3f_2\sin^2(k_x x)\right], \tag{16a}$$

$$\boldsymbol{F}_{\mathrm{ac}}^{\mathrm{calib}} = 2k_x U_{\mathrm{o}}\left[\frac{5\gamma-2}{2\gamma+1} - \frac{1}{\gamma\beta^2}\right]\sin(2k_x x)\,\boldsymbol{e}_x. \tag{16b}$$

The potential $U_{\mathrm{ac}}^{\mathrm{calib}}$ is shown in Fig. 8(a).

If a particle is subject to a Stokes drag force F_{drag} from a flow in the x-direction, then the critical flow velocity v^*, where the acoustic radiation force no longer can trap the particle is given by the condition $F_{\mathrm{drag}} = \max\{|\boldsymbol{F}_{\mathrm{ac}}^{\mathrm{calib}}|\}$ or

$$6\pi\eta a v^* = 2k_x U_{\mathrm{o}}\left[\frac{5\gamma-2}{2\gamma+1} - \frac{1}{\gamma\beta^2}\right]. \tag{17}$$

If v^* is measured experimentally, we are therefore able to determine the acoustic energy scale U_{o} by

$$U_{\mathrm{o}} = 3\pi\frac{\eta a v^*}{k_x}\left[\frac{5\gamma-2}{2\gamma+1} - \frac{1}{\gamma\beta^2}\right]^{-1}. \tag{18}$$

We propose a specific chip design which supports a pressure eigenmode close to the one depicted in Fig. 8(a). The idea is to fabricate an $\alpha = 3$ chip. In such a chip a strong pressure eigenmode of odd symmetry exists in the channel as the $\alpha = 1$ chip in Fig. 5(a) but it will also have a strong anti-node in the silicon as the $\alpha = 2$ chip in Fig. 5(b). Now, if two auxiliary side channels parallel to the first channel is placed at these anti-nodes, the pressure mode inside these side channels is very close to the wanted mode of Fig. 8(a). The correctness of this line of reasoning is proved by numerical simulation of the eigenmodes in such a triple-channel $\alpha = 3$ chip as shown in Fig. 8(b).

5. CONCLUDING REMARKS

By theoretical and numerical analysis we have studied the applicability of the widely used transverse half-wavelength picture. We have shown that, although not entirely correct, this picture is accurate enough to be useful. Furthermore, we have shown that it is crucial to take the entire geometry of the chip into account and match the dimensions of the surrounding silicon to those of the water channel, i.e. a global wave picture must be employed. Finally, we have presented two examples of applying this global wave picture: (*i*) a many-channel chip, which by correct matching performs significantly better in terms of amplitude and homogeneity of the acoustic energy density, and (*ii*) a three-channel chip, which enables *in situ* calibration of the acoustic radiation force.

ACKNOWLEDGMENTS

We thank Thomas Laurell and Per Augustsson at Lund University for many illuminating discussions.

REFERENCES

1. L.V. King, *Proc. R. Soc. London, Ser. A* **147**, 212 (1934).
2. K. Yosioka and Y. Kawasima, *Acustica* **5**, 167 (1955).
3. L.P. Gorkov, *Sov. Phys. Doklady* **6**, 773 (1962).
4. K. Yasuda, S. Umemura, and K. Takeda, *Jpn. J. Appl. Phys.* **34**, 2715 (1995).
5. K. Yasuda, K. Takeda, and S. Umemura, *Jpn. J. Appl. Phys.* **35**, 3295 (1996).
6. J. Spengler and M. Jekel, *Ultrasonics* **38**, 624 (2000).
7. M. Saito, N. Kitamura and M. Terauchi, *J. Appl. Phys.* **92**, 7581 (2002).
8. M. Wiklund, P. Spégel, S. Nilsson and H. M. Hertz, Ultrasonics **41**, 329 (2003).
9. J.F. Spengler, W.T. Coakley, and K.T. Christensen, *AIChE J.* **49**, 2773 (2003).
10. L. A. Kuznetsova and W. T. Coakley, *J. Acoust. Soc. Am.* **116**, 1956 (2004).
11. H. Li and T. Kenny, *Conf. Proc. 26 Ann. Int. Conf. IEEE Engineering in Medicine and Biology*, **3**(4), 2631 (2004).
12. M. Bengtsson and T. Laurell, *Anal. Chem.* **378**, 1716 (2004).
13. J. J. Hawkes, R. W. Barber, D. R. Emerson and W. T. Coakley, *Lab Chip* **4**, 446 (2004).
14. A. Nilsson, F. Petersson, H. Jonsson, and T. Laurell, *Lab Chip **4***, 131 (2004).
15. H. Jonsson, C. Holm, A. Nilsson, F. Petersson, P. Johnsson, and T. Laurell, *Ann. Thoracic Surgery* **78**, 1572 (2004).
16. T. Lilliehorn, U. Simu, M. Nilsson, M. Almqvist, T. Stepinski, T. Laurell, J. Nilsson, S. Johansson, *Ultrasonics* **43**, 293 (2005).
17. S. M. Hagsäter, T. G. Jensen, H. Bruus, and J. P. Kutter, *Lab Chip* **7**, 1336 (2007).
18. S. M. Hagsäter, A. Lenshof, P. Skafte-Pedersen, J. P. Kutter, T. Laurell and H. Bruus, *Lab Chip* **8**, 1178 (2008).
19. O. Manneberg, S.M. Hagsäter, J. Svennebring, H.M. Hertz, J.P. Kutter, H. Bruus, M. Wiklund Ultrasonics **49**, 112-119 (2009).
20. J. Svennebring, O. Manneberg, P. Skafte-Pedersen, H. Bruus, and M. Wiklund Biotechnol. Bioeng. **103**, 323 (2009).
21. J. Lighthill, *Waves in fluid*, (Cambridge University Press, Cambridge, 2005).
22. H. Bruus, "Acoustofluidics" in *Theoretical Microfluidics*, (Oxford University Press, Oxford, 2008).